High-accuracy Brillouin frequency shift measurement system based on stimulated Brillouin scattering phase shift

Yongqian Li
Qi An
Xiaojuan Li
Lixin Zhang

SPIE.

High-accuracy Brillouin frequency shift measurement system based on stimulated Brillouin scattering phase shift

Yongqian Li, Qi An,* Xiaojuan Li, and Lixin Zhang
North China Electric Power University, College of Electrical and Electronic Engineering, Baoding, China

Abstract. A high-accuracy Brillouin frequency shift (BFS) measurement system for vector Brillouin optical time-domain analysis-based temperature sensor is proposed, in which double sideband modulation is used and the stimulated Brillouin scattering (SBS) gain and loss processes work together to generate a superimposed SBS phase-shift spectrum. The measurement principle is analyzed by mathematical modeling and the proof-of-concept experiment is performed by using a 100-m long standard single-mode fiber. The theoretical and experimental results reveal that the temperature sensitivity of BFS obtained from the measured SBS phase-shift spectrum is 1.059 MHz/°C, and the measurement error of temperature is only half that in traditional single sideband-based system, which indicates that the proposed technique can realize high-accuracy temperature measurement and have huge potential in the field of long-distance and high-accuracy sensing. © *The Authors.* *Published by SPIE under a Creative Commons Attribution 3.0 Unported License. Distribution or reproduction of this work in whole or in part requires full attribution of the original publication, including its DOI.* [DOI: 10.1117/1.OE.56.5.056102]

1 Introduction

Stimulated Brillouin scattering (SBS) in silica fiber is described as a nonlinear interaction between two counter-propagating optical waves with a frequency difference of Brillouin frequency shift (BFS) mediated through an acoustic wave, which not only transfers energy between these two optical waves but also changes their phases.[1] Brillouin optical time-domain analysis (BOTDA) sensors based on SBS interaction have gained much attention over the world since 1989,[2] owing to its superiority in distributed monitoring of temperature or strain in km-long fibers at a submeter resolution.[3–7] The measurement of temperature or strain in conventional BOTDA sensor is based on the linear relationship between the BFS and temperature or strain, and the BFS is usually measured by scanning the gain or loss spectrum of SBS amplitude and locating the peak value of the spectrum. Unfortunately, the measurement accuracy in the amplitude spectrum-based system is limited by pump depletion and nonlocal effect.[8–11] In recent years, however, the vector BOTDA (VBOTDA) system capable of measuring both the amplitude and phase-shift spectra of SBS response is introduced by Dossou et al.,[12] and is used to feature the high-order acoustic resonances that are not clear on the SBS amplitude spectrum, by the SBS phase-shift spectrum. Since the temperature- or strain-induced BFS change results in a frequency shift of the SBS phase-shift spectrum, and the BFS can be measured by scanning the SBS phase-shift spectrum and locating its zero point, the SBS phase shift is also applied in BOTDA sensor to measure temperature or strain. A BOTDA sensor employing optical self-heterodyne detection and synchronous demodulation achieved a distributed phase-shift measurement over a 25-km long fiber and

a 10.75-dB enhancement of signal-to-noise ratio (SNR).[13] Since the SBS phase shift is independent of SBS amplitude, it is immune to nonlocal effect, which indicates a huge potential for enhanced long-haul distributed sensors.[14] With the assistance of Raman amplification, VBOTDA-based sensor reduced significantly the relative intensity noise and showed very attractive application prospects in long-range distributed measurements.[15] Xiaobo et al.[16] successfully measured the Brillouin gain and phase-shift spectra by VBOTDA technique employing IQ demodulation and obtained the temperature dependence of Brillouin gain and phase-shift spectra.

To improve the system's performance, unlike the existing VBOTDA system in which only a single sideband (SSB) is used, we propose a BFS measurement system for VBOTDA-based temperature sensor, in which double sideband (DSB) modulation is used and the SBS gain and loss processes work together to generate a superimposed SBS phase-shift spectrum and to achieve a double measurement accuracy. The temperature measurement error of the system is first evaluated mathematically, then a proof-of-concept experiment is performed by using a 100-m long standard single-mode fiber (SMF), and finally, the performances of the proposed DSB BFS measurement system and traditional SSB BFS measurement system for VBOTDA-based temperature sensor are compared.

2 Principle

The principle of the proposed DSB BFS measurement technique for VBOTDA-based temperature sensor is illustrated in Fig. 1. The technique relies on the SBS interaction between probe wave and two pump waves. The frequencies of the two pump waves are symmetrically up- and down-shifted from the frequency of probe wave by ν_p that are tunable in the vicinity of the BFS ν_B. Pump wave 1 acting

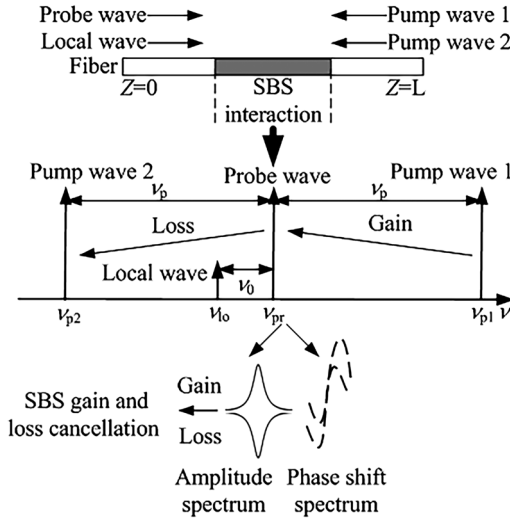*Address all correspondence to: Qi An, E-mail: an-qi.122@163.com

Fig. 1 Schematic diagram of the DSB BFS measurement technique.

as the anti-Stokes wave induces an SBS gain response on the probe wave, whereas pump wave 2 acting as the Stokes wave induces an SBS loss response on the probe wave.

The heterodyne detection for measuring the SBS amplitude and phase-shift responses is realized by introducing a coherent local wave propagating together with the probe wave along the fiber in the same direction. The local wave is away from the probe wave by ν_0 and outside the Brillouin scattering spectra of pump waves; therefore, it does not interact with the pump waves via SBS interaction. The modified steady-state SBS coupled wave equations are described as[17]

$$\frac{dI_{p1}}{dz} = -\alpha I_{p1} - \frac{g_0 \cdot \Delta\nu_B^2}{(4\Delta\nu^2 + \Delta\nu_B^2)} I_{p1} I_{pr}, \quad (1)$$

$$\frac{dI_{p2}}{dz} = -\alpha I_{p2} + \frac{g_0 \cdot \Delta\nu_B^2}{(4\Delta\nu^2 + \Delta\nu_B^2)} I_{p2} I_{pr}, \quad (2)$$

$$\frac{dI_{pr}}{dz} = \alpha I_{pr} + \frac{g_0 \cdot \Delta\nu_B^2}{(4\Delta\nu^2 + \Delta\nu_B^2)} (I_{p2} - I_{p1}) I_{pr}, \quad (3)$$

$$\frac{d\phi_{pr}}{dz} = -\frac{2 \cdot g_0 \cdot \Delta\nu \cdot \Delta\nu_B}{(4\Delta\nu^2 + \Delta\nu_B^2)} (I_{p1} + I_{p2}), \quad (4)$$

where I_{p1} and I_{p2} denote, respectively, the intensities of pump waves 1 and 2 in the fiber, I_{pr} is the intensity of probe wave, α is the fiber attenuation coefficient, g_0 is the peak value of Brillouin gain, $\Delta\nu_B$ is the Brillouin linewidth, $\Delta\nu = (\Delta\nu' - \nu_B)$ is the detuning parameter in which $\Delta\nu'$ is the frequency difference between probe wave and pump wave, and ϕ_{pr} is the phase shift of probe wave.

In Eqs. (1)–(4), the probe wave is assumed to travel in the $+z$ direction, and the pump waves 1 and 2 in the $-z$ direction. Considering that for a practical BFS measurement system, a very small probe wave power is usually used to avoid pump depletion,[11] therefore, to simplify the analysis, it is reasonable to assume that since the power of probe wave is much lower than those of pump waves 1 and 2, the power change of the two pump waves induced by SBS interaction is

so small comparing to their initial level that the pump depletion is negligible and their powers remain approximately equal over the interaction length Δz, defined as the spatial resolution of a sensing system. In this case, the second term on the right-hand side of Eq. (3) vanishes, which indicates that the probe power is not affected by the SBS processes due to the cancellation of SBS gain and loss on the amplitude of probe wave. However, the total phase shift ϕ_{pr} experienced by the probe wave becomes the sum of the phase-shift responses induced by the two SBS interaction processes, which can be deduced by integrating Eq. (4) over the interaction length Δz of the fiber and expressed as Eq. (5), since the parameters concerned are independent of scattering location in the fiber under given conditions:

$$\phi_{pr}(\nu_B, T) = -\frac{2 \cdot g_0 \cdot \Delta\nu \cdot \Delta\nu_B}{(4\Delta\nu^2 + \Delta\nu_B^2)} \cdot \frac{2P_p \cdot \Delta z}{A_{eff}} = 2\phi'_{pr}(\nu_B, T), \quad (5)$$

where $P_p = I_p \times A_{eff}$ denotes the power of the pump wave, in which I_p is the intensity of pump wave in the traditional SSB BFS measurement system, A_{eff} is the effective interaction area of fiber, and ϕ'_{pr} denotes the phase shift in traditional SSB system. In giving Eq. (5), the assumption of the same BFS ν_B in DSB system and SSB system is used, since ν_B is only related to the fiber material for an input light with a given wavelength. As depicted in Fig. 1, the gain and loss responses work together on the probe wave so that the amplitude response of probe wave is kept constant, but the phase-shift response is doubled under the condition of the same P_{p1} and P_{p2}.

In the traditional SSB BFS measurement system, when a phase measurement instrument with an error of $\delta\phi$ is used, the measurement error of BFS in the system can be given by

$$\delta\nu_B^S = \frac{d\nu_B}{d\phi'_{pr}} \delta\phi. \quad (6)$$

For the proposed DSB BFS measurement system, however, when the same measurement method and instrument are used, the measurement error of BFS in DSB system can be written as follows:

$$\delta\nu_B^D = \frac{d\nu_B}{d\phi_{pr}} \delta\phi. \quad (7)$$

From Eqs. (5) and (6), Eq. (7) can be rewritten as follows:

$$\delta\nu_B^D = \frac{1}{2} \cdot \frac{d\nu_B}{d\phi'_{pr}} \delta\phi = \frac{1}{2} \cdot \delta\nu_B^S. \quad (8)$$

Again, since the temperature sensitivity of BFS in the two systems, $C_{\nu T}$, is only dependent on the fiber material, the measurement error of temperature in the proposed system can be expressed as

$$\delta T^D = \frac{\delta\nu_B^D}{C_{\nu T}} = \frac{1}{2} \cdot \frac{\delta\nu_B^S}{C_{\nu T}}, \quad (9)$$

which shows clearly that the temperature measurement error in DSB system is intrinsically only half that in the SSB system.

To evaluate further the measurement error of BFS in the proposed system, the ratio of the phase-shift range to frequency range between the maximum and minimum of the phase-shift spectrum, namely the maximum frequency sensitivity of the phase shift, can be used. From the equation obtained by setting the derivative of Eq. (5) to be zero, when $\Delta\nu = \Delta\nu_B/2$, the maximum of the phase-shift spectrum is obtained as

$$\max(\phi_{pr}) = \frac{P_p}{A_{eff}} \cdot \Delta z \cdot g_0, \tag{10}$$

when $\Delta\nu = -\Delta\nu_B/2$, the minimum of the phase-shift spectrum is obtained as follows:

$$\min(\phi_{pr}) = -\frac{P_p}{A_{eff}} \cdot \Delta z \cdot g_0. \tag{11}$$

According to Eqs. (10) and (11), although the phase-shift range becomes twice that in the SSB system, the corresponding frequency range is kept to be $\Delta\nu_B$, which is the same as that in the SSB system. So, the maximum frequency sensitivity of phase shift can be given by

$$S_{\phi f}^D = \frac{d\phi_{pr}}{d\nu_B} = \frac{2P_p}{A_{eff}} \cdot \Delta z \cdot g_0 \cdot \frac{1}{\Delta\nu_B} = 2\frac{d\phi_{pr}'}{d\nu_B} = 2S_{\phi f}^S, \tag{12}$$

and Eq. (9) can be rewritten as follows:

$$\delta T^D = \frac{\delta\phi}{S_{\phi f}^D \cdot C_{\nu T}} = \frac{1}{2} \cdot \frac{\delta\phi}{S_{\phi f}^S \cdot C_{\nu T}}. \tag{13}$$

The heterodyne detection signal at frequency ν_0 in the DSB system can be expressed as

$$i(\nu_0) = RE_{pr}E_L \cos(2\pi\nu_0 t - \phi_{pr}), \tag{14}$$

where E_{pr} and E_L are the amplitude of the optical field of the probe wave and local wave, and R is the responsivity of photoelectric detector (PD). From Eq. (14), the SBS phase shift and amplitude information can be extracted by heterodyne detection.

3 Experimental Setup

The experimental setup of the proposed DSB BFS measurement technique is depicted in Fig. 2. The continuous wave output of a laser operating at a 1550.057-nm wavelength and with a 10-KHz linewidth is divided into two branches by a polarization-maintaining (PM) coupler. In the upper branch, the optical wave is launched into an electro-optic modulator (EOM) biased at null point and driven by a microwave generator, to produce a DSB suppressed carrier (SC) wave with 22-dB suppression. The two sidebands acting as pump waves 1 and 2 are amplified by an erbium-doped fiber amplifier (EDFA) and extracted from the EDFA output by an optical filter composed of a circulator and a Bragg grating with a center wavelength of 1550.055 nm and a bandwidth of 0.312 nm. The pump waves are passed through a polarization scrambler (PS) to reduce polarization-induced fluctuations and launched by a circulator into a length of standard SMF used as a test fiber. The lower branch is used as a probe wave and is input to a Mach–Zehnder interferometer (MZI) in which the lower arm is used to generate the local wave through a 200-MHz down-shifted acousto-optic frequency shifter (AOFS), and the upper arm is used to adjust the polarization of the probe wave through a polarization controller (PC) to ensure the maximum visibility of the beat signal of the probe wave and local wave. The probe wave and local wave are recombined by coupler 2, the upper output of which is directed to the test fiber through an optical isolator (ISO) that is used to ensure unidirectional transmission, and the lower output of which is detected by PD1 and is used as the reference signal of phase measurement. The probe wave, interacted with the pump waves through SBS interaction, and the local wave from port 3 of circulator 2 are detected by PD2 and used as the detection signal. Finally, the two heterodyne signals are captured by a digital oscilloscope (OSC). The reference signal, detection signal without SBS interaction, and detection signal with SBS interaction can be expressed, respectively, as

$$I_R(\nu_0) = R_1\sqrt{P_{pr}P_L}\cos(2\pi\nu_0 t), \tag{15}$$

$$I'(\nu_0) = R_2\sqrt{P_{pr}P_L}\cos(2\pi\nu_0 t - \phi_f), \tag{16}$$
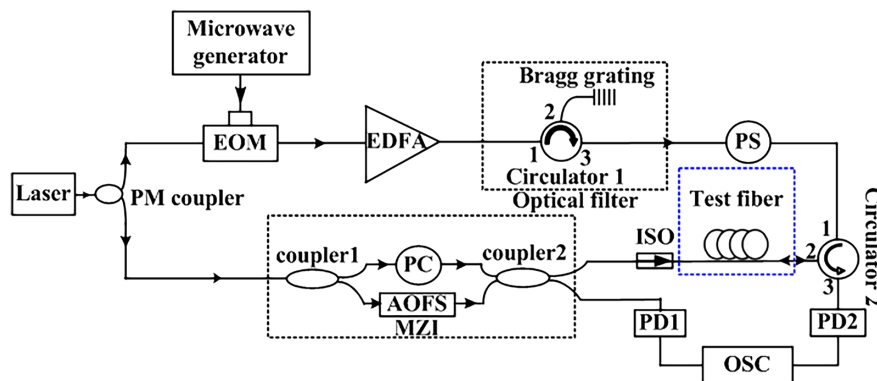

Fig. 2 Experimental setup (PM coupler, polarization maintaining coupler; EOM, electro-optic modulator; EDFA, erbium-doped fiber amplifier; PS, polarization scrambler; PC, polarization controller; AOFS, acousto-optic frequency shifter; MZI, Mach–Zehnder interferometer; ISO, isolator; PD, photoelectric detector; OSC, oscilloscope).

$$I(\nu_0) = R_2 \sqrt{P_{\text{pr}} P_{\text{L}}} \cos(2\pi\nu_0 t - \phi_{\text{f}} - \phi_{\text{pr}}), \qquad (17)$$

where R_1 and R_2 are, respectively, the responsivity of PD1 and PD2, and ϕ_{f} is the phase shift induced by fiber transmission. According to Eqs. (15)–(17), the SBS phase shift ϕ_{pr} can be obtained by subtracting the phase difference ϕ_{f} between the detection signal without SBS interaction and the reference signal from the phase difference $\phi_{\text{pr}} + \phi_{\text{f}}$ between the detection signal with SBS interaction and the reference signal. On the other hand, the SBS amplitude response can be obtained simply by taking the ratio of measured amplitude of the detection signal with SBS interaction to that without SBS interaction. Furthermore, the phase-shift spectrum and amplitude spectrum can be obtained by changing the frequency of the microwave generator. The fiber connectors connected to the circulator and ISO are angle polished to minimize the Fresnel reflections at the fiber ends.

When the center wavelength and bandwidth of Bragg grating in the optical filter are changed to 1549.967 and 0.296 nm, only the pump wave 1 can be extracted, and the SSB BFS measurement system based on SBS gain response can be achieved, which is expected to be used for performance comparison between the DSB system and the SSB system. The detection signal with SBS interaction in the SSB system can be approximately expressed as follows:[13]

$$I(\nu_0) = (1 + g_{\text{SBS}})R_2 \sqrt{P_{\text{pr}} P_{\text{L}}} \cos(2\pi\nu_0 t - \phi_{\text{f}} - \phi'_{\text{pr}}). \qquad (18)$$

4 Results and Discussions

A proof-of-concept experiment of the proposed DSB BFS measurement technique is performed following the setup in Fig. 2, and the SBS phase shift and amplitude spectra of the DSB and SSB systems are compared. The powers of the probe wave and local wave are set to be −5.23 and −3 dBm, respectively; the power of pump waves 1 and 2, i.e., two sidebands of the DSB-SC wave, is fixed to 17.78 dBm, and the sampled heterodyne signals are averaged 1024 times to improve the SNR. A 100-m long standard SMF is used as the test fiber and immersed loosely in a temperature-controlled water tank with the water temperature increasing from 10°C to 80°C by a step of 10°C, and the frequency of the microwave generator is changed from 10.752 to 10.952 GHz with a step of 4 MHz. The frequency sweeping and data sampling are started after having been kept at each temperature for 10 min to ensure the temperature uniformity of the fiber. Three separate measurements for SBS phase shift and amplitude spectra are averaged and fitted by the minimum root mean square method, as shown in Fig. 3.

In Fig. 3, it is seen that the SBS phase shift and amplitude spectra move toward higher frequency when the water temperature increases. The variation of the SBS phase shift and amplitude peak is mainly owing to the power variation of the pump waves. Figure 3(a) shows clearly that the phase-shift range from the maximum to minimum of the SBS phase-shift spectrum in the DSB system is almost twice that in the SSB system at the same operational parameters, which indicates that the maximum frequency sensitivity of the phase shift in the vicinity of BFS can be improved by almost 100% in DSB system. Figure 3(b) illustrates clearly that compared with the
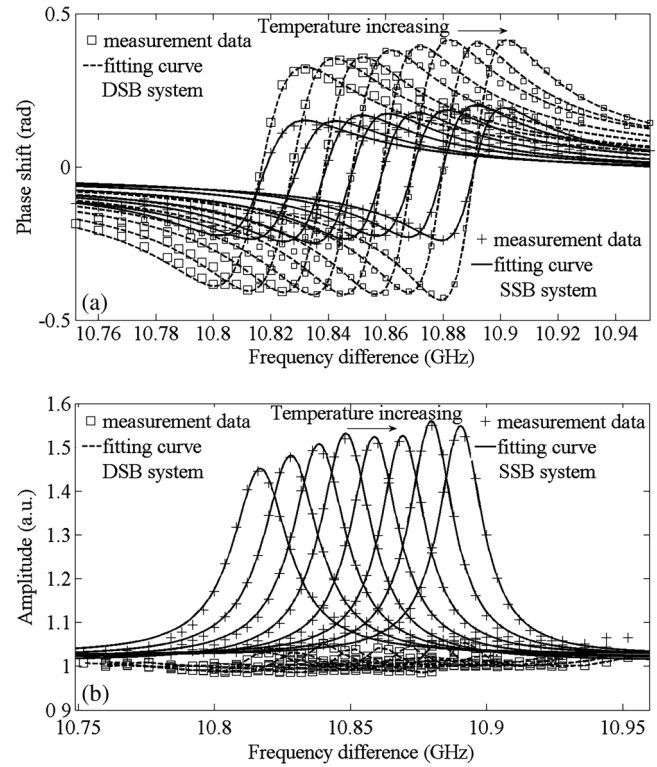

Fig. 3 Measured SBS response spectra at different temperatures employing the DSB system and SSB system: (a) phase-shift spectra and (b) amplitude spectra. The horizontal axis represents the frequency difference between the pump wave and probe wave, which is equal to the frequency of the microwave generator.

SSB system, the probe power is almost unaffected by the SBS processes in the DSB system, which is consistent with the above theoretical analysis and indicates that the non-local effect induced by the energy accumulation on the probe wave transferred between the pump wave and probe wave through SBS interaction[8,9] can be effectively reduced in the proposed system. The small but visible fluctuation of probe power in Fig. 3(b) is induced by the slight inconsistency between P_{p1} and P_{p2} due to equipment limitations.

Figure 4 shows the temperature dependencies of the BFSs obtained by fitting the SBS phase-shift spectra in DSB system and SSB system. It is seen that the measurements in both systems exhibit very good linearity and consistency, and the temperature coefficients are estimated to be 1.059 and
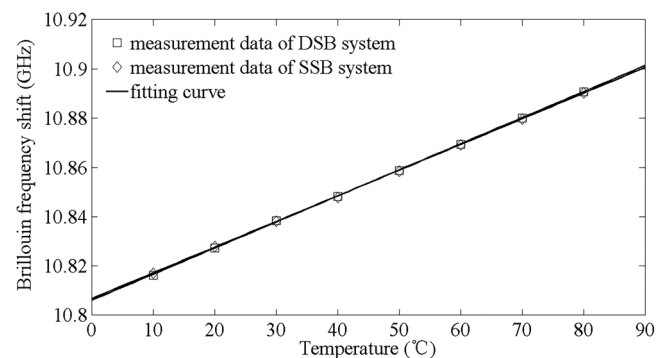

Fig. 4 Temperature dependencies of BFS obtained from the SBS phase-shift spectra in the DSB system and SSB system.
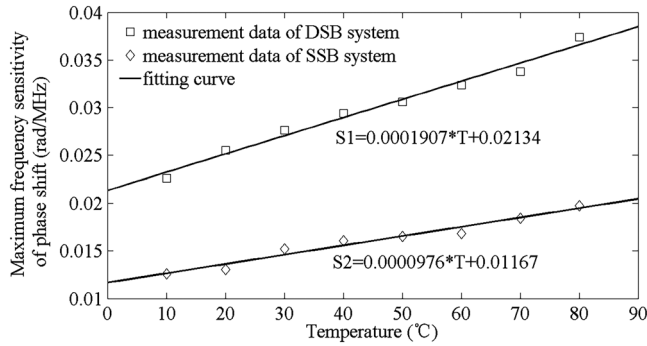
Fig. 5 Maximum frequency sensitivity of phase shift at different temperatures in the DSB system and SSB system.
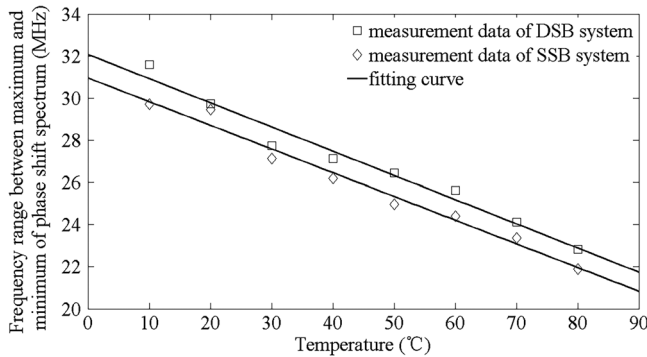

Fig. 6 Frequency range obtained from the SBS phase-shift spectra at different temperatures in the DSB system and SSB system.

1.043 MHz/°C through linear fitting, which demonstrates an excellent sensing performance of the proposed technique.

To demonstrate the high-temperature measurement accuracy of the proposed technique experimentally, the maximum frequency sensitivity of the phase shift is obtained by taking the ratio of phase-shift range to the frequency range between the maximum and minimum of phase-shift spectrum, as shown in Fig. 5. From Fig. 5, the maximum frequency sensitivity of the phase shift increases with the increase of temperature, and the maximum frequency sensitivity of the phase shift in the DSB system is almost twice that in the SSB system, which shows that the measurement error of temperature in the proposed system can be reduced to only half that in SSB system, which is also well depicted in Eqs. (5)–(13).

To clarify the temperature dependence of the maximum frequency sensitivity of the phase shift, the relationships between frequency range $\Delta\nu_B$ and temperature in the two systems are also obtained by the measured phase-shift spectrum, as shown in Fig. 6. It is seen that the frequency range decreases with the increase of temperature in both systems, which is in good agreement with the results reported in the literature,[18] thereby causing the increase of maximum frequency sensitivity with the increase of temperature, as depicted in Eq. (12). But the frequency range in the DSB system is slightly larger than that in the SSB system, which might be also induced by the slight inconsistency between P_{p1} and P_{p2} due to equipment limitations.

It is worth mentioning that since the BFS is proportional to fiber strain, the theoretical and experimental results about measurement error in this paper should be also applicable to fiber strain measurement by the proposed technique. In this case, the strain measurement error can be given as

$$\delta\varepsilon^D = \frac{\delta\phi}{S_{\phi f}^D \cdot C_{\nu\varepsilon}} = \frac{1}{2} \cdot \frac{\delta\phi}{S_{\phi f}^S \cdot C_{\nu\varepsilon}}, \qquad (19)$$

where $C_{\nu\varepsilon}$ is the strain sensitivity of BFS in the two systems, which is also dependent only on the fiber material.

Although the proof-of-concept experiment for temperature sensing in this paper is conducted with continuous probe and pump waves injected into 100-m long fiber due to equipment limitations, the obtained results are equivalent to those from a 1-μs-width pulse pump injected VBOTDA-based temperature sensor; therefore, the spatial resolution of the proposed system can be estimated to be better than 100 m according to the relationship between system spatial resolution and sensing pulse width in a distributed optical fiber sensing system, and a DSB VBOTDA-based temperature sensing system with practical significance can be realized by inserting another EOM driven by a pulse generator between the microwave generator driven EOM and the EDFA, and by replacing the OSC with a data acquisition card and a computer in Fig. 2.

5 Conclusions

We have proposed and demonstrated a high-accuracy DSB SBS phase-shift based BFS measurement technique for VBOTDA-based temperature sensor. The measurement error of the technique has been evaluated mathematically and a proof-of-concept experiment has been implemented by using a 100-m long SMF. The theoretical and experimental results show that the temperature dependence of the BFS is of excellent linearity with a sensitivity of 1.059 MHz/°C, the measurement error of temperature in the proposed DSB system is only half that in traditional SSB system, and the probe wave is almost unaffected by the SBS interaction. The proposed technique can achieve high-accuracy temperature measurement and reduce nonlocal effect, which may lead to a performance-enhanced distributed sensor and new applications.

References

1. G. P. Agrawal, *Nonlinear Fiber Optics*, Academic Press, New York, United States (2008).
2. T. Horiguchi and M. Tateda, "BOTDA-nondestructive measurement of single-mode optical fiber attenuation characteristics using Brillouin interaction: theory," *J. Lightwave Technol.* **7**(8), 1170–1176 (1989).
3. X. Bao and L. Chen, "Recent progress in distributed fiber optic sensors," *Sensors* **12**(7), 8601–8639 (2012).
4. J. Hu et al., "A BOTDA with break interrogation function over 72 km sensing length," *Opt. Express* **21**(1), 145–153 (2013).
5. X. Zhang, J. Hu, and Y. Zhang, "A hybrid single-end-access BOTDA and COTDR sensing system using heterodyne detection," *J. Lightwave Technol.* **31**(12), 1954–1959 (2013).
6. W. Lin et al., "Differential Brillouin fiber sensor based on phase difference on double-sideband pump wave," *Opt. Eng.* **54**(6), 067101 (2015).
7. Q. Sun et al., "High-accuracy and long-range Brillouin optical time-domain analysis sensor based on the combination of pulse prepump technique and complementary coding," *Opt. Eng.* **55**(6), 066125 (2016).

8. E. Geinitz et al., "The influence of pulse amplification on distributed fibre-optic Brillouin sensing and a method to compensate for systematic errors," *Meas. Sci. Technol.* **10**(2), 112–116 (1999).
9. A. Minardo et al., "A reconstruction technique for long-range stimulated Brillouin scattering distributed fibre-optic sensors: experimental results," *Meas. Sci. Technol.* **16**(4), 900–908 (2005).
10. L. Thevenaz, S. F. Mafang, and J. Lin, "Impact of pump depletion on the determination of the Brillouin gain frequency in distributed fiber sensors," *Proc. SPIE* **7753**, 775322 (2011).
11. L. Thevenaz, S. F. Mafang, and J. Lin, "Depletion in a distributed Brillouin fiber sensor: practical limitation and strategy to avoid it," *Proc. SPIE* **7753**, 7753A5 (2011).
12. M. Dossou, D. Bacquet, and P. Szriftgiser, "Vector Brillouin optical time-domain analyzer for high-order acoustic modes," *Opt. Lett.* **35**(22), 3850–3852 (2010).
13. A. Zornoza, M. Sagues, and A. Loayssa, "Self-heterodyne detection for SNR improvement and distributed phase-shift measurements in BOTDA," *J. Lightwave Technol.* **30**(8), 1066–1072 (2012).
14. J. Urricelqui, M. Sagues, and A. Loayssa, "BOTDA measurements tolerant to non-local effects by using a phase-modulated probe wave and RF demodulation," *Opt. Express* **21**(14), 17186–17194 (2013).
15. X. Angulo-Vinuesa et al., "Raman-assisted vector Brillouin optical time domain analysis," *Proc. SPIE* **8794**, 87943A (2013).
16. T. Xiaobo et al., "Vector Brillouin optical time-domain analysis with heterodyne detection and IQ demodulation algorithm," *IEEE Photonics J.* **6**(2), 6800908 (2014).
17. M. Pagani et al., "Tunable wideband microwave photonic phase shifter using on-chip stimulated Brillouin scattering," *Opt. Express* **22**(23), 28810–28818 (2014).
18. X. Bao, J. Smith, and A. Brown, "Temperature and strain measurements using the power, line-width, shape and frequency shift of the Brillouin loss spectrum," *Proc. SPIE* **4920**, 311–322 (2002).

Yongqian Li received his BE degree in electronic instrument and measurement technology and his MS degree in communication and electronic systems from Tianjin University, China, in 1982 and 1988, respectively. He received his PhD degree at Gunma University, Japan, in 2003. Since 2004, he has been a professor in the Department of Electronics and Communication Engineering, North China Electric Power University. His research interests include optical communication and distributed optical fiber sensing.

Qi An received her BE degree in communication engineering from Hebei University of Science and Technology in 2009, and she is now a PhD student in North China Electric Power University with the major of electrical information technology. Her research interests include optical communication and distributed optical fiber sensing.

Xiaojuan Li received her BE degree in electronic and information engineering from Hebei University of Economic and Business in 2009, and she is now a PhD student in North China Electric Power University with the major of electrical information technology. Her research interests include optical communication and distributed optical fiber sensing.

Lixin Zhang received her BE degree in electronic information science and technology from North China Electric Power University in 2011, and she is now a PhD student in North China Electric Power University with the major of electrical information technology. Her research interests include optical communication and distributed optical fiber sensing.